Available online at www.sciencedirect.com
SCIENCE DIRECT
Catalysis Today 114 (2006) 72–85
CATALYSIS TODAY
www.elsevier.com/locate/cattod

Monolith and TAP reactor studies of NO_X storage on $Pt/BaO/Al_2O_3$: Elucidating the mechanistic pathways and roles of Pt

Karen S. Kabin, Pranav Khanna, Rachel L. Muncrief, Vinay Medhekar, Michael P. Harold *

Department of Chemical Engineering, University of Houston, 4800 Calhoun, S222 Engineering Building 1, Houston, TX 77204-4004, USA

Available online 24 March 2006

Abstract

The multiple roles of Pt are examined during NO and NO_2 storage in the presence of O_2 on a series of $Pt/BaO/Al_2O_3$ catalysts spanning 0–3.7 wt.% Pt and employing both a bench-scale monolith and TAP (Temporal Analysis of Products) reactor system. Pt enhances the storage of both NO and NO_2, although the extent of enhancement diminishes at higher Pt loadings. The promotional effect of Pt observed even for short-time NO_2 storage suggests the importance of a Pt–Ba couple and associated spillover processes. During short-time exposure, NO and NO_2 in O_2 store at comparable rates, suggesting the formation of barium mono nitro species in close proximity to Pt. At longer exposure times deeper nitration occurs, apparently involving Ba sites further removed from Pt. NO and NO_2 TAP pulsing experiments reveal coupled NO/NO_2 decomposition and storage on a pre-reduced catalyst which, as oxygen accumulates on the surface, evolves to a storage-only process. A phenomenological storage model is proposed that integrates previous theories from the literature in an attempt to reconcile the observed effects of Pt and the similarities and differences in NO and NO_2 storage. The trends in the data are consistent with the concurrent pathways of NO_X storage; specifically, the ''nitrite'' and ''disproportionation'' pathways, both of which have been proposed in the literature.

Keywords: NO_X; Diesel; Lean-burn; NO_X storage and reduction; Pt; BaO

1. Introduction

NO_X storage and reduction (NSR) is emerging as a viable NO_X emission abatement technology for lean burn and diesel vehicles. First proposed by Toyota researchers, the 'lean NO_X trap' (LNT) is an adsorptive catalytic monolith reactor requiring periodic operation [1,2]. In the first step, exhaust NO_X is adsorbed onto the alkali oxide function of a bifunctional supported precious metal based catalyst. In the second step the stored NO_X is released/reduced by exhaust reductants, achieved by intermittent rich engine operation or fuel injection into the exhaust. Several studies of NSR have demonstrated high time-averaged NO_X conversion (exceeding ca. 80%) on model alumina-supported catalysts containing precious metal (e.g. Pt, Rh) and storage component (e.g. BaO, zeolite) [1–10]. High NO_X conversion is achieved with a sequence of a ca. 30–60 s lean storage period and a ca. 2–10 s rich period [5–10]. By comparison, the conversion obtained for steady state lean NO_X reduction typically does not exceed 50–70% and has a much narrower temperature operating window [11–13].

The NSR reaction system involves a rich array of catalytic and adsorption chemistries that must be individually probed to build a comprehensive understanding of the mechanism and predictive kinetic model. A review by Epling et al. [14] summarizes the emerging understanding of the storage and reduction kinetics and materials that have been studied. A large number of studies have focused on the NO_X storage process on model $Pt/BaO/Al_2O_3$ powder and monolith catalysts [15–38]. Below we summarize the main findings as a backdrop to the current study.

The storage of NO_X on Ba-containing catalyst is such that at temperatures and space velocities of interest, specifically in the ranges 200–400 °C and 20,000–60,000 h^{-1} (monolith support) storage times are typically less than ca. 2–3 min in duration. Times longer than this result in an unacceptable fraction of NO/NO_2 breaking through, which would represent a conversion

* Corresponding author. Tel.: +1 713 743 4307; fax: +1 713 743 4323.
E-mail address: mharold@uh.edu (M.P. Harold).

0920-5861/$ – see front matter
doi:10.1016/j.cattod.2006.02.004

loss during storage and reduction cycling. Thus, the longer-term storage process is only of fundamental interest, whereas the effectiveness of short-term NO_X uptake is of paramount importance. During such short exposure times the utilization of the barium compound is typically less than 10%, with NO_X storage in the range of ca. 1×10^{-4} to 5×10^{-4} mole NO_X/g catalyst. The storage of both NO and NO_2 in O_2 are relevant since NO oxidation to NO_2 occurs readily on the precious metal function of the bifunctional material. The dynamic storage capacity exhibits a maximum value at an intermediate temperature in the range of 300–400 °C. The maximum becomes more pronounced at longer storage times and is thought to be the result of a kinetic limitation at low temperature and of nitrite/nitrate reversible decomposition at high temperature. NO_X storage may also occur on the alumina support at lower temperature.

Uptake of NO and NO_2 in O_2 reveals the existence of multiple regimes and multiple sites on $Pt/BaO/Al_2O_3$. The so-called disproportionation mechanism has been considered by many to be the key underlying route for storage. NO, contained in an O_2/N_2 feed, stores by the sequential oxidation of NO to NO_2 followed by the gas–solid reaction between NO_2 and BaO: $3NO_2 + BaO \rightarrow Ba(NO_3)_2 + NO$. The evolution of NO during NO_2 storage provides evidence for the disproportionation. In this mechanism Pt is involved only during the oxidation of NO with the product NO_2 storing as surface and bulk barium nitrate. Fridell et al. [17] speculated that Pt serves as a source of oxygen adspecies, formed by dissociative adsorption, which enhances the uptake of NO in the presence of O_2 via a spillover mechanism. Research by Anderson and coworkers [26,27] lends support to a more involved role of Pt, such as the enhanced formation of bulk barium nitrate and decomposition of barium carbonate, which is the primary non-nitrogen containing barium species in the presence of CO_2 and hydrocarbons. At short times it has been reported that NO evolution resulting from disproportionation is considerably below the stoichiometric value (NO formed/NO_2 consumed = 0.33), whereas at longer storage times several have reported close agreement [24,25,28]. Epling et al. [28] speculated that the lack of agreement at short times is due to storage on so-called ''alpha'' storage sites that are in close proximity to Pt. A potential explanation is the participation of oxygen adspecies provided by the dissociative adsorption of molecular oxygen on Pt. This oxygen serves to oxidize intermediate surface NO_X species such as nitrites, which have been detected by IR surface spectroscopy. Scotti et al. [25] showed that the model developed by Olsson et al. [19] can account for the variance from the disproportionation stoichiometry. Specifically, the NO_2 is postulated to first form a nitro-barium intermediate, $BaONO_2$, which then decomposes, liberating NO and forming BaO_2. It is not until the deeper nitration achieved with the sequential addition of two additional NO_2 molecules that the overall disproportionation stoichiometry is satisfied. Schmitz and Baird [31] have proposed a similar mechanism in which a mixture of nitrites and nitrates is formed during the initial exposure of BaO to NO_2. Subsequent addition of more NO_2 liberates NO and produces nitrates.

A second proposed pathway involves the initial adsorption of NO_2, forming a nitro-bound species such as the aforementioned $BaONO_2$. Subsequent addition of NO_2 leads to the formation of a mixture of nitrites and nitrates, as well as barium peroxide, BaO_2. Hess and Lunsford [32,33] detected BaO_2 with Raman spectroscopy during the exposure of NO_2 to BaO supported on MgO. They proposed a similar mechanism which involved first the formation of an intermediate nitro species, followed by a mixture of nitrites and nitrates upon further exposure to NO_2. In the presence of O_2 their data also showed evidence for BaO_2 formation with subsequent conversion to nitrates during NO_2 exposure. The oxidation of BaO competed with NO_2 storage during the initial stages of storage. Stone et al. [35] observed evidence for BaO_2 formation during exposure of a Ba covered Pt surface to gas phase O_2.

A third pathway has been proposed by Prinetto et al. [23] and Nova et al. [24] to explain the uptake of NO in O_2 and have coined it the ''nitrite route''. Their mechanistic proposal requires a more demanding coupling between the Pt and Ba. Initial uptake of NO_X leads to storage as barium nitrites, which upon deeper oxidation by molecular O_2 leads to barium nitrate. This picture is supported by in situ IR data which show the growth and depletion of bands characteristic of nitrites during sustained exposure to NO/O_2 at ca. 350–400 °C [23]. Pt serves as a promoter of nitrite formation and oxidation in addition to its catalytic role in NO oxidation to NO_2.

Previous studies have reported that while the initial uptake of NO/NO_2 is relatively fast, the uptake rate slows considerably. Earlier studies attributed the two rate regimes to surface and bulk barium. Tuttles et al. [36] attribute this to the onset of diffusion limitations at the level of the barium particle. Muncrief et al. [37] described using a simple model that while complete barium nitration is feasible at lower temperatures (ca. 500 °C for BaO; <300 °C for $BaCO_3$) a significant fraction of the barium is kinetically inaccessible because of diffusion limitations. TGA data corroborate a picture in which the accessible barium oxide or carbonate is nitrated, which because of particle densification or washcoat pore plugging inhibits further storage.

The objective of the current study is to further elucidate the role of Pt during NO and NO_2 storage on a series of model $Pt/BaO/Al_2O_3$ catalysts. We focus on short exposure (storage) times for which the breakthrough of NO_X is minimized. We also compare the storage features of NO to NO_2, both in excess O_2, since in practice the oxidation of NO on Pt ensures that a fraction of the NO_X storage is contributed by the NO_2. We employ both a bench-scale monolith reactor and TAP (Temporal Analysis of Products) reactor system to monitor the transient uptake of NO and NO_2. To this end, we analyze and interpret the monolith and TAP results with the aforementioned mechanistic storage models.

2. Experimental

2.1. Monolith reactor system

The monolith catalysts used for these experiments were provided by Engelhard Corporation. Larger cylindrical cores

(D = 3.8 cm, L = 7.6 cm) were cut using a dry diamond saw to a smaller cylindrical shape (ca. D = 0.8 cm, L = 2 cm, mass of washcoat ~0.1 g). The smaller monoliths were then wrapped in Fiberfrax® ceramic paper that had been heat treated and then placed in a quartz tube reactor. The samples contained varying amounts of Pt and BaO on a γ-alumina washcoat support adsorbed on a cordierite structure (~62 channels/cm^2). The compositions of the catalysts are given in Table 1, B0–B4. The catalyst surface area was measured using N_2 adsorption–desorption at 77 K with the BET method. Engelhard Corporation provided measurements of the Pt dispersion, Pt surface area and average Pt diameter. The Pt dispersion was estimated from CO chemisorption measurements at 35 °C, after reduction in H_2 at 400 °C, and assuming a 1:1 CO/Pt ratio. The catalyst characteristics listed in Table 1 were performed using powder samples with compositions identical to the monolith washcoat.

The experimental set-up utilized is shown in the top panel of Fig. 1 and is similar to the one described in previous studies [8,9,38]. The major components of this set-up included a gas supply system, a reactor system, an analysis system, and a data acquisition system. The gas supply system utilized a series of gas cylinders (Matheson Tri-Gas) and mass flow controllers (MFC) to simulate lean exhaust conditions. One set of mass flow controllers (MKS Inc.) were used to feed the reactive gases (NO, NO_2, O_2, bal. N_2), while the other set of MFCs were used for pure N_2. Both of these gas streams were continually fed at 1 standard liter per minute (slpm) and mixed using an in-line static mixer prior to entering the reactor system. The reactor system consisted of a four-port, dual-actuated switching valve installed immediately upstream of the reactor, and a quartz tube flow reactor positioned inside a Mellen SC11 tube furnace. The switching valve was used to alternate between the feed streams instead of adjusting the MFC set points. A needle valve was placed on the vent line to hold a back pressure on the feed gas stream exiting to the vent in order to minimize pressure fluctuations. The reactor and furnace temperatures were monitored with several K-type thermocouples. The thermocouple utilized for these experiments measured the catalyst temperature (T_c). It was positioned within an internal monolith channel at the approximate mid-point of the monolith (radial and axial). After the reactor system, the effluent gases flowed through heated lines (110 °C) to a gas phase analysis system composed of a FT-IR spectrometer, O_2 analyzer and THC analyzer (Total Hydrocarbon Analyzer), as described by Muncrief et al. [8]. The species detected in the FT-IR included NO, NO_2, N_2O, NH_3, CO, CO_2, H_2O, and C_3H_6.

The data acquisition system consisted of two PCs and an ADAM 500 TCP module. Analog signals from the thermocouples, the pressure gauge, the analyzers, the switching valve, and the mass flow controllers were sent to an ADAM 5000 TCP module (Advantech) to convert the signals from analog to digital. This data was then recorded using one PC while the FT-IR composition data was collected on a separate PC. In order to synchronize the two time stamps, at the end of the storage experiment a dilute propylene feed was pulsed over the catalyst while the catalyst temperature was maintained at 525 °C. The time stamp differential can be accurately determined by lining up the recorded position of the switching valve and the FT-IR propylene measurement. This same time stamp differential was then used to determine the precise time of the NO and NO_2 injection.

For all of the monolith experiments, the catalyst temperature and total flow rate were fixed at 340 ± 5 °C and 1 slpm, respectively, and the feed composition was either 500 ppm NO with 5% O_2 in a balance of nitrogen (NO + O_2 feed) or 500 ppm NO_2 with 5% O_2 in a balance of nitrogen (NO_2 + O_2 feed). Prior to performing a set of storage experiments, the catalyst was first stabilized by cycling between a hydrocarbon lean and hydrocarbon rich feed gas for ca. 6 h at an inert feed temperature of ca. 325 °C. After the stabilization process, the catalyst temperature was raised to 525 °C. Five 30-s pulses of 3000 ppm propylene were injected, followed by a 10-min feed containing 5% oxygen. The catalyst temperature was then reduced back to 340 °C before commencing with the storage experiment. After the storage was complete, the NO or NO_2 was shut off and the reactor temperature was ramped back up to 525 °C (this temperature corresponded to a 550 °C inert feed temperature). At the elevated temperature, the propylene pulses were injected again in order to have multiple reference points and ensure that the data still lined up. After this, the reactor was cooled back down in N_2 and more cycling experiments were performed.

Some barium carbonate is likely to have formed during the propylene injection time-stamping procedure. However, we expect that the rather high temperature (525 °C) and the subsequent treatment in O_2/N_2 minimized the extent of carbonate at the commencement of storage experiments. We observed during the O_2/N_2 feed a temporal production of CO_2, which we believe to be the product of barium carbonate decomposition and oxidation of carbonaceous species on the catalyst.

Table 1
Listing of catalysts used in study and their properties

Catalyst sample	Pt (wt.%)	BaO (wt.%)	Pt dispersion (%)	Pt surface area (m^2/g)	Pt particle size (nm)	BET area (m^2/g)
B0	0.00	16.7	n/a	n/a	n/a	107
B1	0.32	16.6	39.8	0.31	2.85	111
B2	1.27	16.5	33.0	1.04	3.43	109
B3	2.20	16.3	21.9	1.19	5.18	116
B4	3.71	16.0	34.7	3.18	3.26	107
B5	0.50	12.0	–	–	–	140

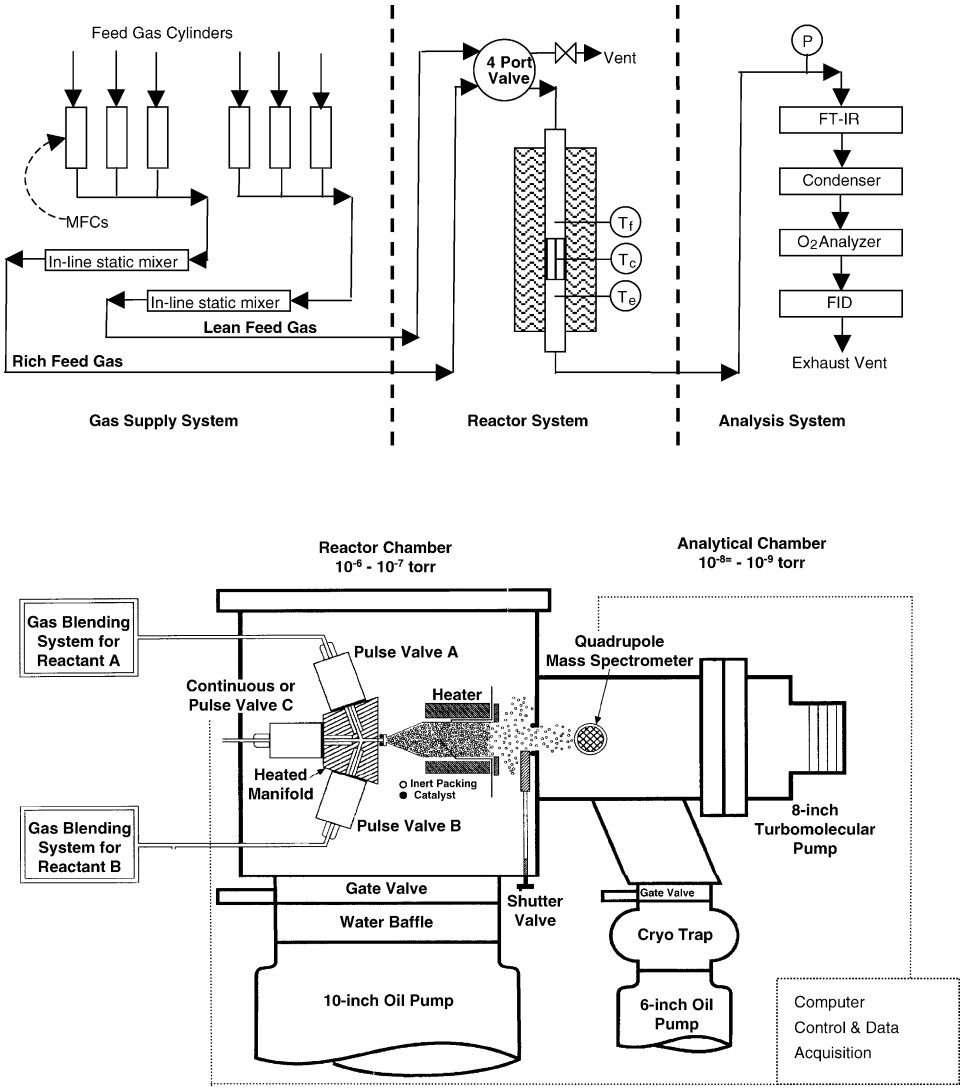

Fig. 1. Schematics of bench-scale monolith reactor system (top panel) and TAP reactor system (bottom panel).

2.2. TAP reactor system

The TAP experiments performed in this work have been carried out in a "TAP-1" reactor system. The TAP method, developed by Gleaves et al. [39], has been employed in many previous catalytic systems which we will not review in detail here. Given that NSR is an inherently transient catalytic process, the TAP is an ideal experimental tool. To our knowledge the TAP has not been applied to NO_X storage and reduction.

The basic working principle of the TAP involves the transient interrogation of a catalyst through various reactant feed protocols, including single reactant pulsing, dual reactant pulsing, and pulsing-probing. A key feature of the TAP is operation at low pressure (ca. 10^{-5} to 10^{-7} Torr), conditions for which the primary gas phase transport process is Knudsen diffusion. While the transient total pressure is higher during the pulsing, a pulse of sufficiently small intensity ensures operation in the Knudsen regime. The ability to quantify the Knudsen transport enables one to isolate chemical from physical rate processes. The TAP affords the ability to measure transient kinetics at prescribed catalyst states. In the context of NSR, this corresponds to extracting kinetics at a precise degree of nitration although in this study the focus is on storage.

The main components of the TAP reactor employed in this study include a reactant feed system, including high-speed pulse valve assembly, a flow-through temperature-controlled catalytic microreactor, a quadrupole mass spectrometer (UTI model 100C) for product gas analysis, and a PC-based data acquisition and control system. A group of diffusion, mechanical, and turbomolecular pumps maintain the system at the desired vacuum. Product gas fluxes are monitored with the QMS. The response of each component is calibrated by correlating the measured ion current at the prescribed amu value with molecular flow rate. The cracking pattern of NO_2 interfered with that of NO at $m/e = 30$. We overcame this by resolving the cracking pattern of NO_2, in which the ratio of the parent fragment at $m/e = 46$ was approximately 25% of the intensity of the fragment at $m/e = 30.1$. This finding was consistent with data reported by the NIST Mass Spectrometer

Data Center [40]. Additional details of the TAP system and procedures are reported in [41].

In the storage experiments in this study, NO and NO_2 were pulsed over the $Pt/BaO/Al_2O_3$ catalyst (B5), 112 mg of which was positioned between sections of quartz beads. The TAP microreactor is a stainless steel cylinder 4.2 cm in length and 0.64 cm in diameter. It is surrounded by a copper sleeve which is wound with a resistance heater and a cooling coil. The catalyst temperature is monitored with a thermocouple placed in the catalyst bed. This thermocouple supplied the signal programmable temperature control of the catalyst temperature. In a typical NO or NO_2 pulse experiment, the catalyst was first pre-reduced by pulsing H_2 at 400 °C for 120 min, followed by pulsing of Ar for 15 min. NO or NO_2 was then pulsed into the catalyst bed at the prescribed catalyst temperature and the responses for the product species were monitored as a function of time. In this study the pulse intensity was in the range of 3×10^{15} to 5×10^{15} molecules/pulse with a duration of 4–5 s. After each run, the catalyst bed temperature was increased to 400 °C and H_2 pulsed for 120 min to remove any surface oxygen or nitrogen species.

3. Results

3.1. NO and NO_2 storage on monolith experiments

Exposure of a mixture of NO/O_2 to the series of monolith catalysts reveals the promoting effect of Pt. As expected, negligible conversion of NO oxidation occurs with the Pt-free catalyst (B0) whereas the catalysts with high Pt loading (B3 and B4) exhibit the highest NO_2 product concentration (see Fig. 2).

The dependence of the trapping efficiency, defined as the percentage of $NO + NO_2$ fed that is stored [38], and NO_2/NO_X effluent concentration ratio on the exposure time and Pt loading for a $NO + O_2$ feed is shown in Fig. 3. The catalysts with >1% Pt loading had significantly improved trapping efficiencies and the NO oxidation conversion approached a steady-state value more rapidly for the catalysts with higher Pt loadings. At short times (<50 s), catalysts B2–B4 had minimal NO_X breakthrough. The NO and NO_2 concentrations measured at these short times were within the error range of the FT-IR, creating ''noise'' in the NO_2/NO_X ratio calculation.

The dependencies of the trapping efficiency, NO effluent concentration, NO_2 effluent concentration, and NO_2/NO_X effluent concentration ratio on the exposure time and Pt loading for a $NO_2 + O_2$ feed are shown in Fig. 4. For the catalysts with the lowest Pt loading (B0, B1, and B2 with 0, 0.32, and 1.27 wt.% Pt, respectively) the initial storage of NO_2 was accompanied by the evolution and release of NO at concentrations greater than equilibrium. This trend was not apparent for any of the catalysts using a feed of $NO + O_2$ and was also not apparent for catalysts B3 and B4 when using $NO_2 + O_2$ as a feed gas.

In order to further elucidate the influence of Pt on the NO_X storage process, the instantaneous and integral ratios of NO evolved/NO_2 consumed were evaluated for the case of

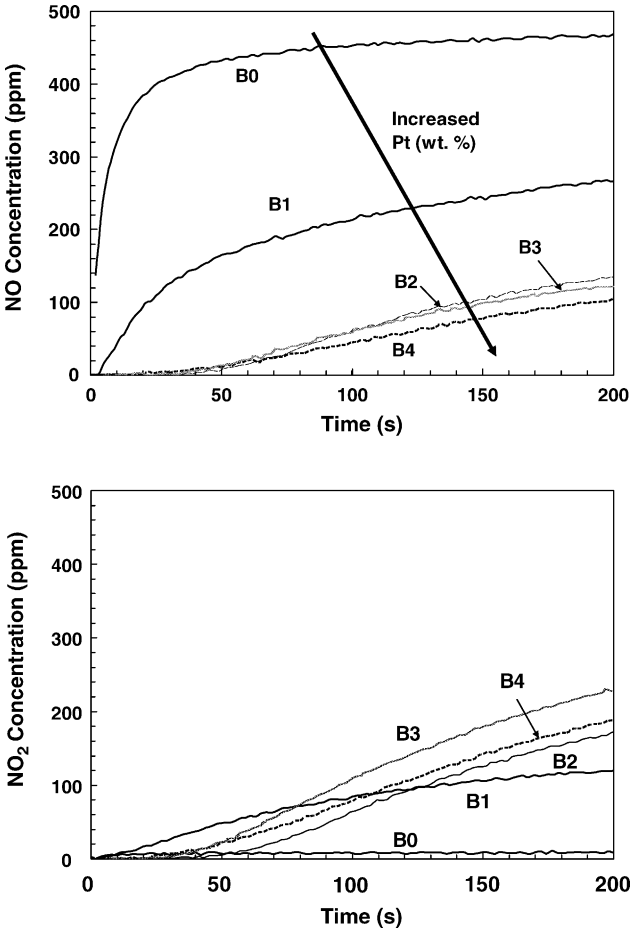

Fig. 2. Dependence of NO and NO_2 effluent concentrations on the exposure time and Pt loading for a feed of 500 ppm NO and 5% O_2 in a balance of nitrogen. The flow rate is 1 slpm and the catalyst temperature is 340 °C.

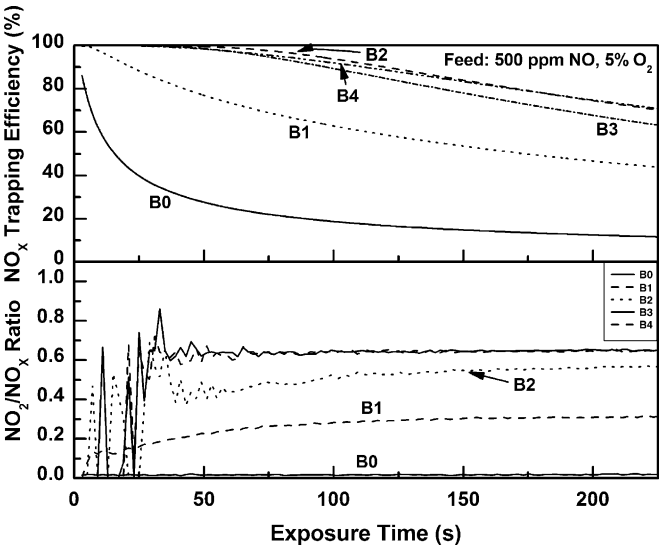

Fig. 3. Dependence of trapping efficiency and NO_2/NO_X effluent concentration ratio as a function of exposure time and Pt loading for a feed of 500 ppm NO and 5% O_2 in a balance of nitrogen. The flow rate is 1 slpm and the catalyst temperature is 340 °C.

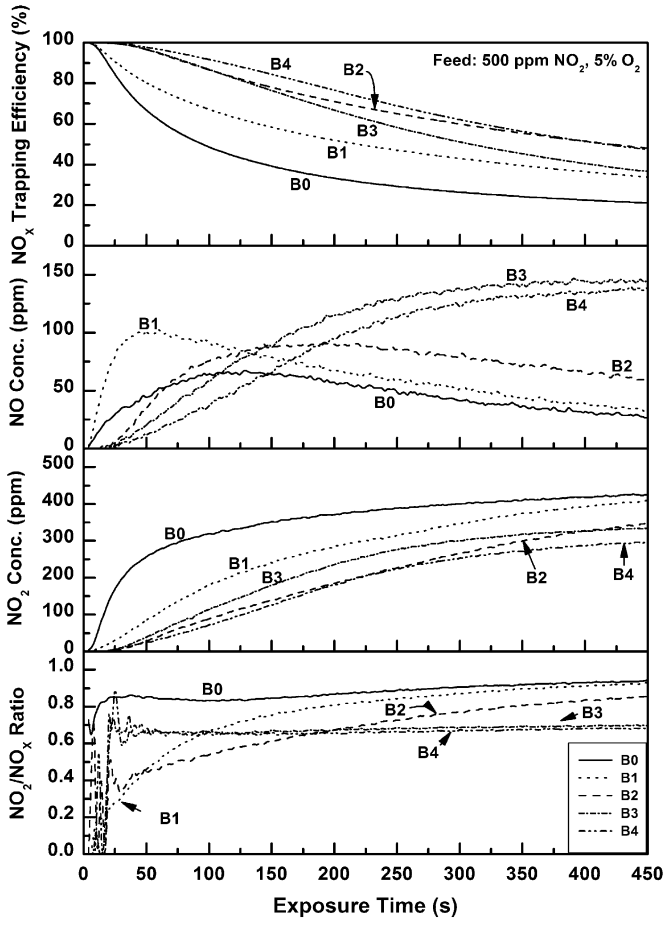

Fig. 4. Dependence of trapping efficiency, NO and NO_2 effluent concentrations, and NO_2/NO_X effluent concentration ratio as a function of exposure time and Pt loading for a feed of 500 ppm NO_2 and 5% O_2 in a balance of nitrogen. The flow rate is 1 slpm and the catalyst temperature is 340 °C.

$NO_2 + O_2$ feed (see Figs. 5 and 6). In these experiments, the instantaneous ratio is defined as:

$$\frac{C_{NO}(t)}{C^{o}_{NO_2}(t) - C_{NO_2}(t)}, \quad (1)$$

where $C^{o}_{NO_2}$ is the inlet NO_2 concentration and C_{NO_2} and C_{NO} are the NO_2 and NO effluent gas concentrations, respectively. The integral ratio is defined as:

$$\frac{\int_0^{t^*} C_{NO}(t)\mathrm{d}t}{\int_0^{t^*} [C^{o}_{NO_2}(t) - C_{NO_2}(t)]\mathrm{d}t}, \quad (2)$$

where $C^{o}_{NO_2}$ is the inlet NO_2 concentration, C_{NO_2} and C_{NO} the effluent gas concentrations, and t^* is the total time. A more detailed analysis of these results is presented in Section 4.

Fig. 7 illustrates the dependence of NO_X storage on Pt loading and exposure time for $NO + O_2$ and $NO_2 + O_2$ feeds. For both NO and NO_2 feeds, the NO_X storage was a monotonic function of exposure time. At short times ($\leq$180 s), the NO_X storage appears to be a monotonically increasing function of Pt loading, but this relationship did not hold true at longer storage times. The nonmonotonic dependence of the longer term storage on the Pt loading was confirmed in repeated runs with

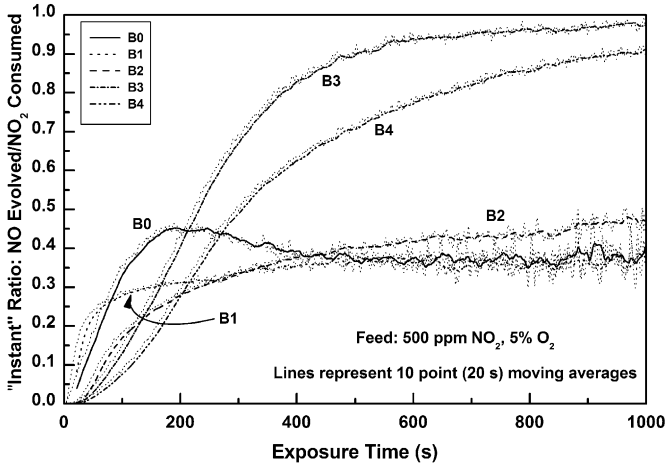

Fig. 5. Instantaneous ratio of NO evolved to NO_2 consumed for the series of catalysts with varied Pt loadings. The flow rate is 1 slpm and the catalyst temperature is 340 °C. Feed gas composition is 500 ppm NO_2, 5% O_2, and balance N_2.

$NO + O_2$ and $NO_2 + O_2$ feeds. The interpretation of this data is presented in more detail later.

The main findings from the storage experiments on the monolith samples are summarized as follows:

i. Pt enhances the storage of NO and NO_2 (in O_2) for Pt loadings less than ca. 1.5 wt.%.
ii. At higher Pt loadings the Pt enhancement effect diminishes and there is little difference in the rates/extents of NO and NO_2 storage.
iii. There is negligible difference between NO and NO_2 (in O_2) at short exposure times (less than ca. 3 min) and nonzero Pt loadings. Under these conditions the disproportionation stoichiometry is not satisfied.
iv. At longer exposure times (exceeding ca. 5 min) and lower Pt loadings (ca. 1.5 wt.%) the storage of NO_2 exceeds that of NO. Under these conditions the disproportionation stoichiometry is satisfied.

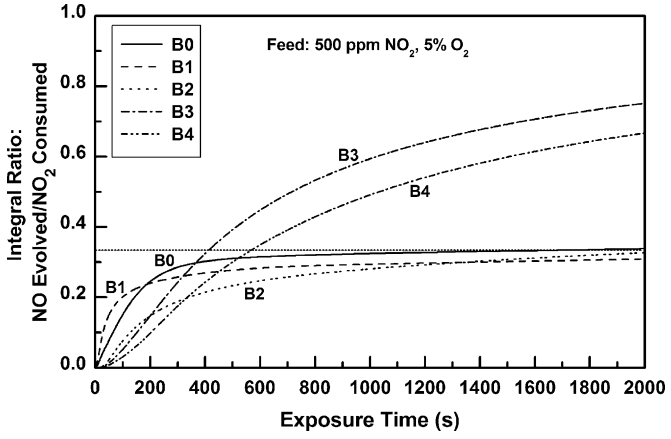

Fig. 6. Integral ratio of NO evolved to NO_2 consumed for series of catalysts with varied Pt loadings. The flow rate is 1 slpm and the catalyst temperature is 340 °C. Feed gas composition is 500 ppm NO_2, 5% O_2, and balance N_2.

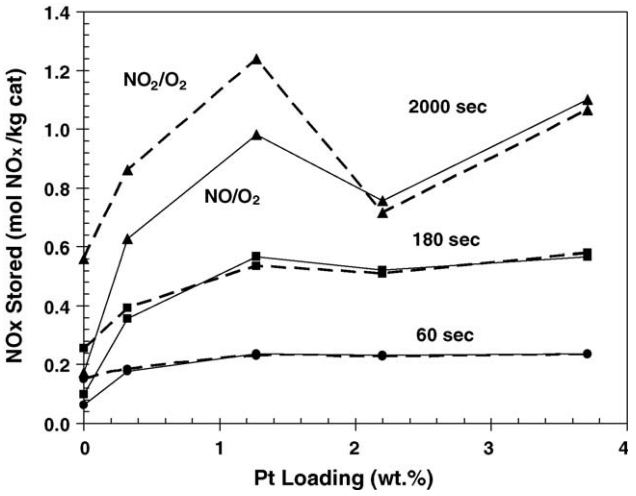

Fig. 7. Dependence of NO_X storage on Pt loading for NO/O_2 and NO_2/O_2 feeds at three different storage times.

v. A noted decrease in storage for both NO and NO_2 was observed at longer exposure times for the catalyst (B3) with a lower Pt dispersion and corresponding higher Pt particle size. The dependence of the effluent $NO_2/(NO + NO_2)$ ratio on the Pt loading is shown in Fig. 8 for the NO/O_2 and NO_2/O_2 feed experiments. The ratio obtained with the NO/O_2 feed increases monotonically while the ratio obtained with the NO_2/O_2 feed decreases monotonically to about the same asymptotic value at high Pt loadings.

3.2. NO pulsing TAP experiments

The results for a typical NO pulsing experiment with a pre-reduced $Pt/BaO/Al_2O_3$ catalyst (B5) are shown in Fig. 9. The molecular flux signals were normalized by their respective maximum values. For comparison to the NO pulse results, the signals for Ar and N_2 are shown from separate Ar and N_2 pulse experiments. Both reactant NO and product N_2 were detected, with the N_2 signal preceding that of NO. When N_2 was pulsed it appeared sooner than the N_2 produced from NO decomposition while the Ar pulse appeared just slightly after the N_2 pulse.

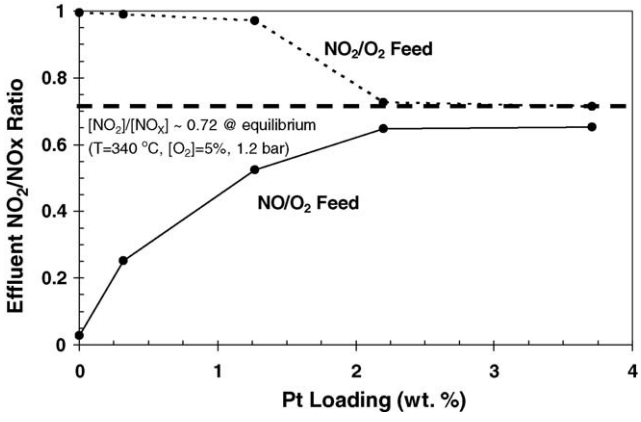

Fig. 8. Dependence of the effluent NO_2/NO_X ratio on the Pt loading for both NO/O_2 and NO_2/O_2 feeds at 340 °C, 5% O_2, and 1.2 bar total pressure.

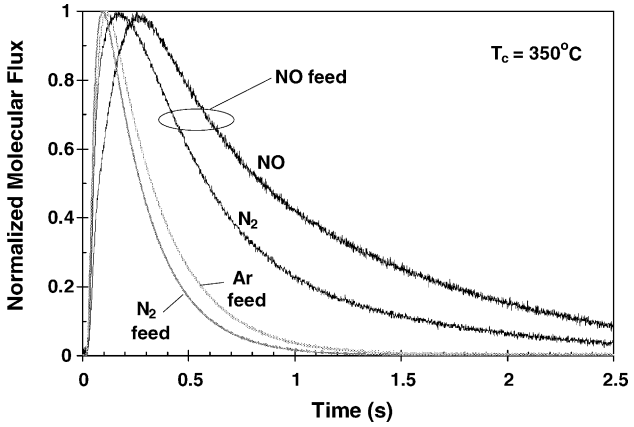

Fig. 9. Typical effluent profiles of tracer Ar, product N_2 and reactant NO vs. time during the pulsing of NO over Pt/BaO/alumina catalyst (B5) at 350 °C.

NO was pulsed over the pre-reduced $Pt/BaO/Al_2O_3$ catalyst maintained at 350 °C. During the course of the NO pulsing experiment the effluent NO and N_2 flux was monitored. Fig. 10 shows the (unreacted) NO effluent profiles at pulse numbers 250, 500, 750, and 1000. The amount of NO (area under the curve) increased with increasing pulse number. Fig. 11 shows the integrated NO and N_2 flux (in molecules/pulse) along the course of a 1000 NO pulse experiment carried out at 350 °C. NO was not detected initially. However, after breakthrough, the NO increased monotonically with pulse number. The product N_2 initially increased, reached a maximum, and then decreased with increasing pulse number.

We have also carried out other NO pulse experiments on Pt sponge and Pt/Al_2O_3 catalysts. N_2O was detected with its yield higher at lower temperatures (<350 °C). The use of supported catalyst can prolong the emergence of effluent species due to pore diffusional effects. These issues will be reported in more detail in a future publication.

3.3. NO_2 pulsing TAP experiments

Similar pulsing experiments were carried out using NO_2 as the reactant. As in the case for NO, we observed N_2 initially and

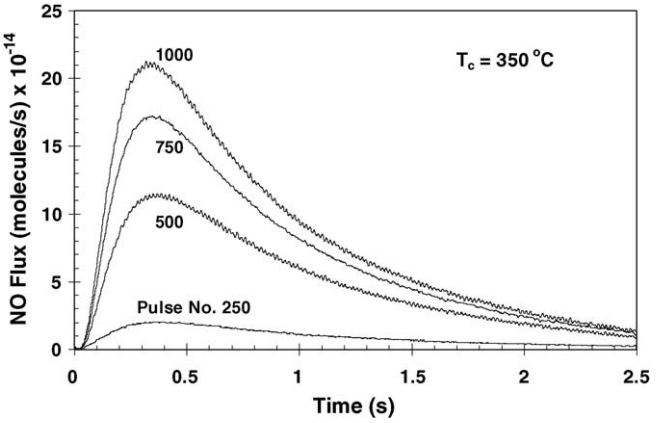

Fig. 10. Typical effluent profiles of reactant NO vs. time during the pulsing of NO over Pt/BaO/alumina catalyst (B5) at 350 °C. Shown are the instantaneous flux profiles at pulse number 250, 500, 750, and 1000.

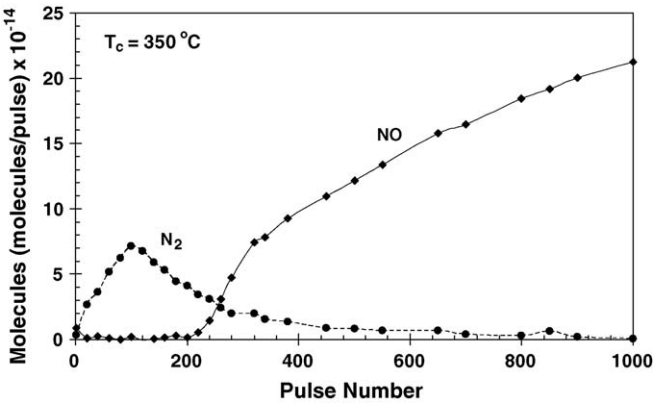

Fig. 11. Effluent profiles of reactant NO vs. time during the pulsing of NO over Pt/BaO/alumina catalyst (B5) at 350 °C. Shown are the instantaneous flux profiles at pulse number 250, 500, 750, and 1000.

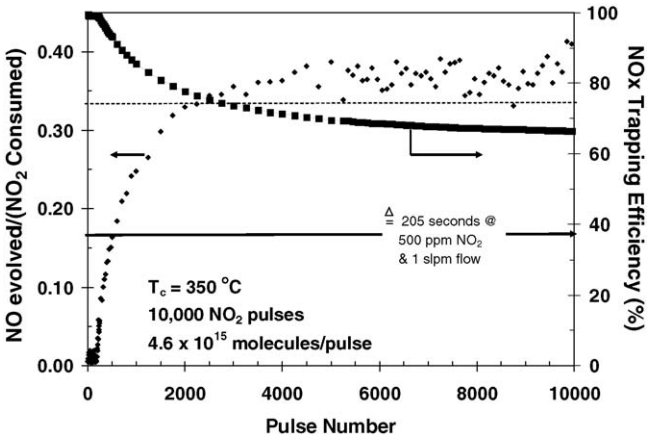

Fig. 13. Instantaneous ratio of NO evolved to NO_2 consumed and NO_X trapping efficiency as a function of NO_2 pulse number. The catalyst (B5) temperature is 350 °C.

did not detect any O_2. After an initial induction period, significant NO was detected while only negligible amounts of NO_2 and N_2O were detected during this series of experiments.

A series of 10,000 NO_2 pulses were fed over the pre-reduced B5 catalyst. The effluent profiles of the first 2000 pulses are shown in Fig. 12. Product N_2 was detected initially, exhibiting a maximum in production at about the 100th NO_2 pulse. The N_2 intensity decreased to the noise level by the 400th pulse. NO was initially not detected, but after breakthrough at ca. 200th pulse the intensity increased monotonically with pulse number. This behavior resembled qualitatively what was observed in the NO pulsing experiments (Fig. 11). The NO effluent profile over the entire 10,000 pulse experiment is shown in Fig. 13. Plotted is the ratio of the molecules of NO produced to the molecules of NO_2 consumed. (The latter quantity corresponds to the NO_2 fed since NO_2 was not detected in the effluent.) This ratio increases rather sharply upon NO breakthrough then increases more gradually after the 2000th pulse, and fluctuates between 0.35 and 0.40 after the 5000th pulse. Also plotted is the trapping efficiency, defined as the percent of NO_X fed that is stored or trapped by the catalyst. (The amount not trapped corresponds to the NO detected in the effluent.)

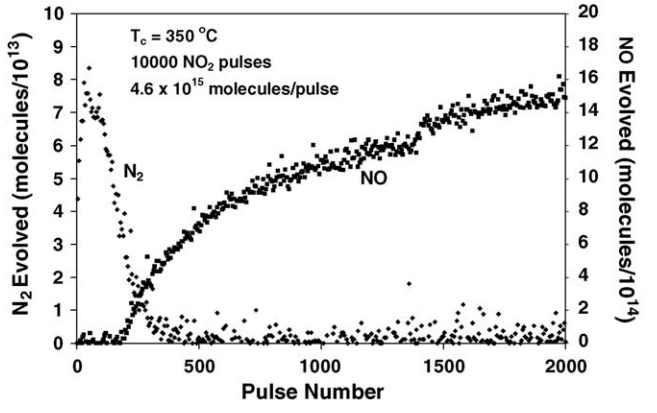

Fig. 12. N_2 and NO production as a function of the NO_2 pulse number. The catalyst (B5) temperature is 350 °C.

4. Discussion

We have carried out a systematic study of the storage of NO and NO_2 over a series of $Pt/BaO/Al_2O_3$ catalysts in monolith and TAP reactor systems. The data provide insight into the kinetics and mechanistic pathways of the storage process, especially at short exposure times, as well as the role of Pt. In this section we analyze the main features of the monolith and TAP data in terms of both kinetic and mechanistic factors.

As a backdrop to the analysis, a phenomenological storage model is proposed that builds on theories posed in the literature and is an attempt to reconcile data from this study and related literature data. A schematic of potential storage pathways for NO and NO_2 on $Pt/Ba/Al_2O_3$ is shown in Fig. 14. The schematic shows four overall reactions (denoted by R1–R4), eight reaction steps (denoted by S1–S8), and three pathways (I–III) from feeds containing NO/O_2, NO_2/O_2, and NO_2. Steps that involve Pt are so indicated. The four overall reactions and associated pathways are as follows:

- R1 is the Pt-catalyzed oxidation of NO to NO_2:

  R1 : $NO + 0.5O_2 \leftrightarrow NO_2$;

  This reaction is the key one for producing NO_2, which can subsequently store via pathways II or III. It is the reversibility of NO oxidation that enables parallel storage pathways to occur from a feed containing only NO/O_2 or NO_2/O_2.
- R2 is the Pt-catalyzed formation of barium nitrate from a mixture of NO and O_2:

  R2 : $BaO + 2NO + 1.5O_2 \leftrightarrow Ba(NO_3)_2$;

  Steps S1–S4 comprise the ‘‘nitrite pathway’’ (I) with the notable features being the close coupling between Pt and Ba, and the involvement of NO and O_2, not NO_2, in the storage process [23,24]. The dissociative adsorption of oxygen in steps S1 and S4 provide oxygen adatoms for the formation of BaO_2 and oxidation of barium nitrite, $Ba(NO_2)_2$, respectively. The formation of the intermediates $BaONO_2$ and barium

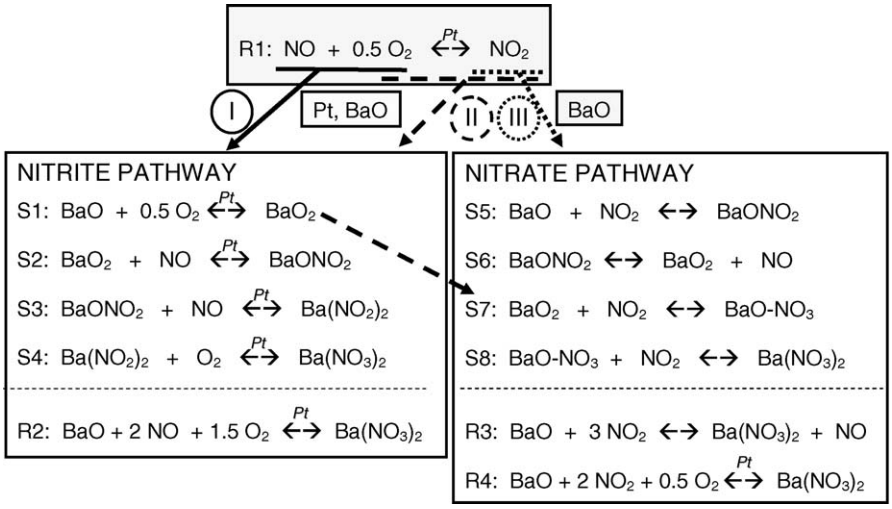

Fig. 14. Schematic of reaction pathways involving feeds containing NO/O_2, NO_2/O_2, and NO_2.

nitrite involves the adsorption and addition of NO to the barium component in close proximity to the Pt.

- R3 is the sequential nitration of BaO by NO_2:

$$R3: \quad BaO + 3NO_2 \leftrightarrow Ba(NO_3)_2 + NO;$$

It is the overall reaction for the ''disproportionation pathway'' (III). Given a feed containing NO_2, barium nitrate formation does not require the direct participation by Pt. The coupling of R1 and R3 has been considered the important pathway for NO_X storage from a NO/O_2 feed. An alternative mechanism was suggested by Hess and Lunsford [32,33] which involves the sequential addition of NO_2, first forming a mixture of barium nitrites and nitrates, and then barium nitrate, while liberating NO:

$$NO_2 + BaO \leftrightarrow Ba(ONO_2)$$

$$Ba(ONO_2) + NO_2 \leftrightarrow \{[Ba(NO_2)]^+ + [BaNO_3]^+\}$$

$$\{[Ba(NO_2)]^+ + [BaNO_3]^+\} + NO_2 \leftrightarrow Ba(NO_3)_2 + NO$$

This mechanism is similar to the nitrate mechanism in its lack of participation by Pt and the initial formation of a nitro species. A subtle difference is the co-formation of nitrate and nitrite intermediate species with the liberation of NO delayed until the addition of the third NO_2 molecule.

- R4 is the Pt-catalyzed formation of barium nitrate from a mixture of NO_2 and O_2:

$$R4: \quad BaO + 2NO_2 + 0.5O_2 \leftrightarrow Ba(NO_3)_2;$$

It is the overall reaction representing a hybrid pathway (II) that involves steps S1, S7, and S8.

With the storage pathways defined, we now analyze the data. The importance of Pt in the storage process was apparent when feeding NO/O_2 to the $Pt/BaO/Al_2O_3$ catalysts, as revealed in Figs. 2 and 3. For the Pt-free Ba/Al_2O_3 sample (B0) the effluent NO increases sharply just after admission of the NO (Fig. 2a) and, expectedly, negligible conversion of NO to NO_2 is achieved (Fig. 2b). The minor amount of storage of NO that occurs has been observed elsewhere [24]. The corresponding trapping efficiency decreases to less than 20% after 200 s. In contrast, Pt loadings exceeding 1 wt.% have notable catalytic and storage-enhancement effects. Complete NO_X trapping occurs by ca. 40–50 s with the trapping efficiency exceeding 80% after 150 s exposure time. Moreover, the NO_2/NO_X effluent ratio, which is a measure of the instantaneous conversion of NO to NO_2, approaches a constant value of ca. 0.70 for the higher Pt loading catalysts (B3 and B4). This is close to the equilibrium NO oxidation fractional conversion of 0.72 at 340 °C. This result suggests that the gas achieves a pseudo-equilibrium even though the slower storage process prevents the achievement of a true steady-state conversion (and equilibrium) until tens of minutes have lapsed. (Data provided elsewhere indicates that more than 2000 s is needed for the NO_X effluent concentration to approach the NO_X feed concentration [38].) Thus, a high Pt loading provides for a rapid conversion of NO to NO_2, which can then store on the BaO via the disproportionation pathway III.

Storage experiments carried out with a NO_2/O_2 feed reveal the combined effects of NO_2 storage and decomposition (Fig. 4). Storage of NO_2 occurs readily even on the Pt-free sample (B0), resulting in a trapping efficiency of 80% at 30 s. The NO effluent profiles exhibits a maximum for the lower Pt loading samples (B0–B2) but increase monotonically for the higher Pt loading samples (B3 and B4). Such trends have been reported elsewhere [24,25,28]. NO is produced by Pt-catalyzed NO_2 decomposition and during barium nitrate formation in the storage process. For the Pt-free sample, the maximum reflects a time-dependent rate of NO_2 storage. With Pt present the NO production is enhanced by NO_2 decomposition. The monotonic increasing NO profile for B3 and B4 reflects a faster NO_2 decomposition. That NO is not immediately detected is likely due to the fact that the Pt is fully oxidized at the start of the storage process. The extent of NO_2 decomposition is evident in the NO_2/NO_X effluent ratio; the higher the Pt loading the more rapid is the approach of this ratio to a constant value. Not coincidentally, the limiting value is ca. 0.70 reflects the establishment of the aforementioned pseudo-equilibrium consistent with the NO/O_2 storage results. The NO_2/NO_X ratio

exceeds 0.70 for the lower Pt loading catalysts because of a reduced rate of NO_2 decomposition.

The relative contribution of the NO_2 storage and decomposition is elucidated by examining the ratio of NO formed/NO_2 consumed (Figs. 5 and 6). The dependence of the instantaneous ratio (Fig. 5) and integral ratio (Fig. 6) are similar to data reported by Nova et al. [24], Scotti et al. [25], and Epling et al. [28]. At the commencement of NO_2 exposure the instantaneous ratio increases from zero and approaches a plateau at or about 0.33–0.40. A value of 0.33 is consistent with the disproportionation stoichiometry:

$$\text{R3}: \quad \text{BaO} + 3\text{NO}_2 \leftrightarrow \text{Ba(NO}_3)_2 + \text{NO}$$

Were nitrate formation immediate, then the instantaneous ratio would achieve a value of 0.33 at the commencement of NO_2 exposure. (This statement assumes that NO oxidation and NO_2 storage occurring downstream of the NO_2 storage front is not significant). This is not the case for any of the catalysts (Figs. 5 and 6). We return to this issue below. If the storage process continues until equilibrium is achieved, at that point the net rate of reaction R3 will approach zero. Our work and the works of others have shown that the approach to equilibrium can be very prolonged due to the slow nitration of bulk BaO [28,37]. At the point when the NO_2 disproportionation rate is negligible, the NO formed/NO_2 consumed ratio will approach a new limit. If the catalyst contains Pt, then the new limit will be unity, which is reflective of the NO_2 decomposition:

$$\text{R1}: \quad \text{NO}_2 \leftrightarrow \text{NO} + 0.5\text{O}_2$$

The trajectory of the ratio obtained for the high Pt loading catalysts (B3 and B4) shows an accelerated approach to unity, indicating a much higher rate of NO_2 decomposition.

All of the catalysts exhibit a gradual increase in the NO formed/NO_2 consumed ratio from zero, with about 400 s of exposure time needed to approach a value in the range 0.33–0.40 (Fig. 5). The rate of increase in the ratio from zero is higher for the catalysts with lower Pt loadings. The Pt-free catalyst (B0) even exhibits a relative maximum in the instantaneous ratio at about 200 s of exposure time. In the sample devoid of Pt (B0) the likely storage route is the disproportion pathway III. However, the deviation of the short-time NO_2 storage data from the disproportionation stoichiometry is consistent with the formation of a NO_X surface species suggested in the recent literature (Epling et al. [28] and Nova et al. [24]). By conducting the NO_2 storage at lower temperature (200 °C), Epling et al. reduced the likelihood of readsorption and oxidation of NO that evolves in the upstream part of the reactor. They conjectured that surface NO_X species on barium sites in close proximity to Pt are oxidized by oxygen adatoms supplied by gas phase oxygen. On the other hand, the model of Olsson et al. [18,19], through simulations carried out by Scotti et al. [25], suggests that the two-step, given by

$$\text{S5}: \quad \text{NO}_2 + \text{BaO} \leftrightarrow \text{BaONO}_2$$

$$\text{S6}: \quad \text{BaONO}_2 \leftrightarrow \text{BaO}_2 + \text{NO},$$

is responsible for the observed trend. A fit of the Olsson et al. model to storage data indicates that the second step of the sequence is rate limiting, with the subsequent addition of two NO_2 molecules occurring rapidly. This mechanism accounts for the delayed evolution of NO during the initial stages of storage. It is also capable of predicting a value of the ratio exceeding 0.33 at short times, noting that S5 and S6 when combined predict a ratio of unity. Moreover, the more rapid increase in the ratio for the catalysts with lower Pt loading is consistent with this mechanism. Finally, the catalysts with the highest Pt loading (B3 and B4) exhibit the most rapid uptake of NO_2 (Fig. 4). That a commensurate rate of increase in the NO formed/NO_2 consumed ratio is not encountered is more consistent with the short-time storage mechanism given by

$$\text{S1}: \quad 0.5\text{O}_2 + \text{BaO} \rightarrow \text{BaO}_2$$

$$\text{S7}: \quad \text{NO}_2 + \text{BaO}_2 \rightarrow \text{BaONO}_3$$

That is, a larger fraction of the NO_2 stores on barium sites that have been oxidized by oxygen adatoms spilling over from Pt crystallites. Indeed, Epling et al. [28] showed a reduction in the rate of NO_2 storage if the gas phase O_2 concentration was reduced.We return to these issues in relation to the TAP experiments below.

The storage behavior of NO and NO_2 on the series of monolith catalysts is summarized in Fig. 7. This figure captures the effect of NO versus NO_2 (in O_2), exposure time, and Pt loading, and provides insight into several mechanistic issues. We consider five key trends that were summarized in Section 3.

i. Pt enhances the storage of NO and NO_2 (in O_2) for Pt loadings less than ca. 1.5 wt.%.

   The Pt-free sample exhibits some storage capacity, but the addition of even a small amount of Pt has a significant effect on the short- and long-term storage. The Pt enhancement of NO storage can be explained by the combination of NO oxidation (R1) and NO_2 storage by the nitrate route (pathway III). Certainly the NO_2 storage on the Pt-free (B0) catalyst is attributed to pathway III. However, the Pt enhancement of NO_2 storage in the presence of O_2 suggests a more direct involvement of Pt in the storage process. The hybrid pathway II that involves dissociative oxygen adsorption on Pt followed by oxidation of BaO to BaO_2 followed by reaction with NO_2 certainly appears plausible.

ii. At higher Pt loadings the Pt enhancement effect diminishes and there is little difference in the rates of NO and NO_2 storage.

   At higher Pt loading the rate of NO oxidation increases, leading to a more rapid establishment of NO oxidation pseudo-equilibrium (i.e. storage still occurring) and true equilibrium (negligible storage rate). Fig. 8 shows the steady-state effluent NO_2/NO_X ratio which is equivalent to the steady-state NO conversion (i.e. no net rate of NO or NO_2 storage). At high Pt loadings the effluent composition is independent of the feed composition (NO or NO_2). Even at long storage times in which steady-state is still not established (e.g. 2000 s) an approach to reaction equili-

brium results in a negligible difference between the extent of NO and NO_2 storage.

iii. There is negligible difference between NO and NO_2 (in O_2) at short exposure times (less than ca. 3 min) and nonzero Pt loadings. Under these conditions the disproportionation stoichiometry is not satisfied.

An examination of the NO and NO_2 effluent concentrations obtained with a NO/O_2 feed (Fig. 2) or NO_2/O_2 feed (Fig. 4) reveals that steady state is not established at 200 s (i.e. $NO + NO_2 < 500$ ppm). Notwithstanding the implied differences in the species concentration profiles along the length of the reactor, the NO and NO_2 uptakes are nearly identical at short times. The NO_2 storage on the Pt-free (B0) catalyst is attributed to pathway III. The incremental increase in NO_2 storage with the addition of Pt and the presence of a high gas phase concentration of O_2 is likely a result of the opening-up of pathway II. In the case of the NO/O_2 feed, the addition of Pt enables the oxidation of NO to NO_2 with subsequent storage via pathway III, although storage by pathways I and II may also occur. However, following the above discussion related to the NO formed/NO_2 ratio, the nearly identical uptakes of NO and NO_2 suggests that storage is primarily $BaONO_2$ or $BaONO_3$ species, respectively. Insufficient time is allowed for deeper nitration to nitrites/nitrates to occur due to rate limitations associated with either pathway. For the disproportionation pathway (III) the limiting step may be the spillover and storage of NO_2 onto nearby BaO sites:

$$NO_2\text{–}Pt + BaO \leftrightarrow BaONO_2 + Pt$$

For the nitrite pathway (II) and hybrid pathway (II) the rate limiting step may be the spillover and reaction of oxygen adspecies with neighboring BaO:

$$O\text{–}Pt + BaO \leftrightarrow BaO_2 + Pt$$

iv. At longer exposure times (exceeding $\leq$5 min) and lower Pt loadings (ca. 1.5 wt.%) the storage of NO_2 exceeds that of NO. Under these conditions the disproportionation stoichiometry is satisfied.

As discussed earlier, at longer storage times the NO_2 disproportionation pathway (III) is clearly important. This helps to explain why the storage of NO_2 exceeds that of NO in the absence of Pt or at longer exposure times. Gas phase NO_2 accesses barium storage sites that are not in close proximity to Pt. For Pt loadings up to 1.5 wt.% there is a nearly constant incremental increase in NO_2 storage, apparently by this route. This bulk nitrate storage is superimposed on storage that proceeds via the Pt/Ba couple (routes I or II).

v. A noted decrease in storage for both NO and NO_2 was observed at longer exposure time for the catalyst with a lower Pt dispersion and corresponding higher Pt particle size.

The nonmonotonic dependence of the NO and NO_2 storage versus Pt loading at the 2000-s storage time and to a lesser extent at the 180-s storage time appear inconsistent with trends and mechanistic explanations to this point. In order to explain the storage minimum encountered with the B3 catalyst (2.2 wt.% Pt) one needs to examine in more detail the catalyst properties (Table 1). The B3 catalyst has a significantly smaller dispersion (21.9%) and larger Pt particle size (5.18 nm) than the other Pt containing catalysts. As noted in previous discussion, the Pt–Ba couple is critical for storage, especially at short storage times and with a NO/O_2 feed. A quantitative measure of the Pt–Ba couple is the interfacial perimeter between the Pt particles and BaO storage component. The specific Pt surface area, a_{Pt} (nm^2/g), and specific Pt perimeter, p_{Pt} (nm interface/g), are respectively given by:

$$a_{Pt} = n_{Pt}\frac{\pi d_{Pt}^2}{4} \tag{3}$$

$$p_{Pt} = n_{Pt}\pi d_{Pt} \tag{4}$$

where d_{Pt} is the average Pt particle size and n_{Pt} is the number of Pt particles per gram of catalyst. If we solve for n_{Pt} in Eq. (4) and substitute into (3) we derive the specific interfacial perimeter, p_{Pt}/a_{Pt}, which is a function of d_{Pt}:

$$\frac{p_{Pt}}{a_{Pt}} = \frac{4}{d_{Pt}} \tag{5}$$

The dependence of the p_{Pt}/a_{Pt} on the Pt loading is shown in Fig. 15. The quantity has a minimum at a loading of 2.2%, reflecting the larger particle size and reduced dispersion for the B3 catalyst.

Keeping with the premise that storage occurs via the Pt/Ba couple and is therefore a function of the interfacial perimeter between Pt and BaO, we can determine the NO_X storage normalized by the interfacial perimeter, $S_{NO_X/Pt}$:

$$S_{NO_X/Pt}\,(\text{atom N/nm interface}) = \frac{NO_X\ \text{storage}\,(\text{atoms N/g cat})}{p_{Pt}\,(\text{nm/g cat})} \tag{6}$$

This quantity provides a measure of how effective is a catalyst in utilizing the Pt/Ba couple for storage. Fig. 15 shows the dependence of $S_{NO_X/Pt}$ on the Pt loading for a 2000 s exposure of NO/O_2. The plot shows that the B3 catalyst (2.2 wt.%) is equally effective in utilizing the Pt/Ba interface as the B2

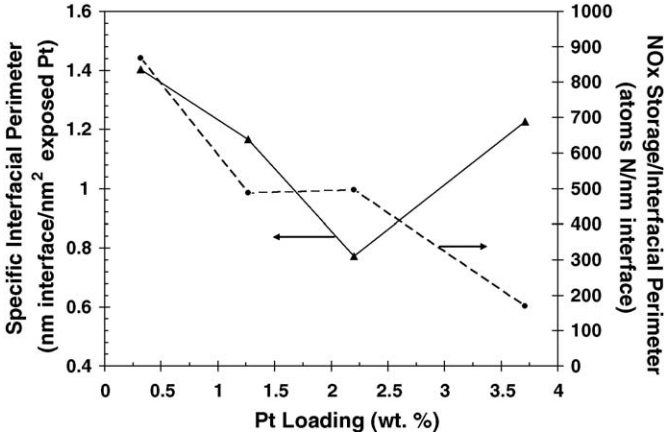

Fig. 15. Dependence of the interfacial perimeter and NO_X storage per interface perimeter on the Pt loading.

catalyst (1.27 wt.%). This result lends credence to the argument that the diminished interfacial perimeter of the B3 catalyst is responsible for the reduced storage. The more general trend indicates that $S_{NO_X/Pt}$ is a decreasing function of the Pt loading. This suggests that the higher Pt loading catalysts are less effective than the lower Pt loading catalysts in utilizing the Pt/Ba couple. That is, added Pt has a diminished enhancement on the storage rate.

One final trend to explain concerns why the reduction in storage encountered with the 2.2 wt.% (B3) catalyst is more pronounced at longer rather than shorter storage times (Fig. 7). Specifically, the percent reduction in the NO_X storage between the B2 and B3 catalyst is 23% at 2000 s, 8% at 180 s, and a negligible 2% at 60 s. This trend is consistent with the picture of a Pt/Ba interface-driven storage process. At shorter times the rate of NO uptake is primarily determined by the supply of NO or NO_2. It is not until longer exposure time has lapsed that the storage becomes limited by the spillover processes at the Pt/Ba interface brought about by the occupation of storage sites in the vicinity of Pt crystallites.

The NO and NO_2 pulsing experiments in the TAP reactor provide a more detailed look at the decomposition chemistry and storage processes that occur on $Pt/BaO/Al_2O_3$.

The NO pulsing experiments confirm key attributes of the reaction pathways. Previous studies have proposed the following mechanism for NO exposure and decomposition over Pt is proposed following previous literature [42–44]:

$$1: \quad NO + Pt \leftrightarrow NO{-}Pt$$

$$2: \quad NO{-}Pt + Pt \leftrightarrow N{-}Pt + O{-}Pt$$

$$3: \quad 2N{-}Pt \leftrightarrow N_2 + 2Pt$$

$$4a: \quad NO{-}Pt + N{-}Pt \leftrightarrow N_2O + 2Pt$$

$$4b: \quad 2NO{-}Pt \leftrightarrow N_2O + O{-}Pt + Pt$$

$$5: \quad 2O{-}Pt \leftrightarrow O_2 + 2Pt$$

The NO pulse experiments are similar to the TAP study reported by Burch and coworkers [43,44] who used a Pt/Al_2O_3 catalyst. Our results are consistent with the Burch et al. data in terms of N_2 and NO effluent measurements, and confirm the steps 1–3 pathway to produce N_2. The lack of observation of product O_2 at the catalyst temperature of 350 °C is consistent with the slow rate of desorption of oxygen adatoms, which has a binding energy of 200–250 kJ/mole. N_2O is an important product at lower temperatures when the NO coverage is higher. The effect of temperature will be explored in more detail elsewhere.

The results from NO pulsing experiments show that the chemical processes can be decoupled from the transport processes (Fig. 9). The response from the pulsing of inerts Ar and N_2 quantify the transport rates through the inert particles and catalyst bed. Both the NO and N_2 pulses from the NO pulse experiments peak after the evolved inerts, quantifying the delay associated with the adsorption, reaction, and desorption steps. TAP reactor modeling is needed to show that the proposed mechanism is consistent with the transient data, and is the subject of an ongoing study.

The local maximum in the production of N_2 and the increase in unreacted NO during NO pulsing is evidence for oxygen adatom inhibition. The recombination of nitrogen adatoms requires sufficiently high nitrogen coverage for reaction 3 to occur. At the start of the experiment on a pre-reduced Pt surface, the N adatom coverage is zero. As NO is pulsed in, NO adsorption (reaction 1) and N–O bond scission (2) occur, increasing both the N and O coverages proportionally. As the surface coverage of nitrogen adatoms increases with pulse number, the rate of N adatom recombination to form N_2 increases. On the other hand, the O adatoms accumulate on the surface as a result of the high desorption energy. This accumulation inhibits reaction 3, and results in a maximum in the N_2 production. (This was also confirmed in independent experiments not reported here in which NO, when pulsed over a pre-oxidized Pt surface, led to no N_2 production [41].) In addition, the O adatom accumulation inhibits the adsorption of NO, leading to an increase in unreacted NO in the effluent.

The effect of the NO_X storage component has a more subtle effect on the results. Burch et al. [43] reported a time delay between the reactant NO pulse and the product nitrogen pulse during the nitrogen monoxide decomposition experiment over a Pt/Al_2O_3 catalyst. More specifically, the reactant NO appeared before the product N_2. A similar time delay was observed in unpublished data from our laboratory during NO pulsing over a Pt sponge catalyst and during more recent NO pulsing experiments over a Pt/Al_2O_3 catalyst [45]. Burch et al. attributed this delay to the series of surface steps involving the conversion of NO to N_2, including adsorption, dissociation, N adatom recombination, and N desorption.

On the other hand, over the $Pt/Ba/Al_2O_3$ catalyst used in this work, the opposite order of evolving species is observed. The product N_2 pulse peaks before the reactant NO pulse. The switch in NO–N_2 peak order suggests an interaction of the NO with the support or storage component. Indeed, in our more recent studies with Pt/Al_2O_3 we have observed that the pulse order is a function of catalyst temperature and the degree of reduction of the catalyst. It is known that NO can store on both Al_2O_3 and BaO. Nova et al. [24] compared the storage of NO in the absence of gas phase O_2 on γ-Al_2O_3, BaO/γ-Al_2O_3, Pt/γ-Al_2O_3, and $Pt/BaO/\gamma$-Al_2O_3. They showed that NO storage increased in that order, although the storage was smaller than in the presence of O_2 (an exception being Al_2O_3 which stored more NO in He than in He + O_2). These issues will be explored in more detail in a forthcoming publication.

A mechanism for NO adsorption on BaO in the absence of O_2 consistent with the data involves the following steps:

$$6: \quad O{-}Pt + BaO \leftrightarrow BaO_2 + Pt$$

$$7: \quad NO + BaO_2 \leftrightarrow BaO{-}NO_2$$

$$8: \quad NO{-}Pt + BaO_2 \leftrightarrow BaO{-}NO_2 + Pt$$

This sequence of steps are consistent with the mechanism posed earlier for NO and NO_2 storage on the monolith catalysts.

Oxygen adatoms from NO decomposition spill over to adjacent BaO sites, forming BaO_2. Gas phase or surface NO can then form the $BaONO_2$ surface species. Previous investigators have proposed similar steps in the context of the storage of NO and NO_2 in the presence of O_2, including Anderson et al. [27] and Nova et al. [24], following the lead of an earlier study by Hess and Lunsford [32,33] who detected the formation of BaO_2 with in situ Raman spectroscopy.

The extent of NO storage is estimated by an overall N balance during the NO pulsing experiments; undetected N is assumed to be stored on the catalyst. At 350 °C and 1000 NO pulses, the amount stored is approximately 4.5×10^{-5} mole N/g cat. This value is consistent with the value of ca. 1×10^{-4} mole N/g reported by Nova et al. [24] for NO (without O_2) exposure to a $Pt/BaO/Al_2O_3$ (1/20/100, w/w). In ongoing work to be reported elsewhere we are investigating the effect of pore diffusion on the storage dynamics which can prolong the residence time of the NO. Thus, the estimated storage may be an over-estimate. In data not reported here, the storage was found to be a decreasing function of temperature over the range 350–450 °C [41], a trend attributed to decomposition of the stored NO_X compound.

Many of the features exhibited in the NO pulsing experiments are evident with NO_2 as the reactant, including N_2 production, oxygen inhibition, and storage. The maximum in N_2 production during the series of NO_2 pulses and the lack of any detected effluent O_2 is more evidence for the same site blockage mechanism. The production of N_2O is determined by the relative rates of N adatom recombination (step 3) and reaction between N and adsorbed NO (step 4a) or the disproportionation of two NO adspecies (step 4b). For example, the ratio of the rates of steps 3 and 4 is proportional to the coverages of N and NO. At lower temperature the NO coverage is higher and therefore N_2O production is favored. This will be presented in more detail elsewhere.

The storage of NO_2 on $Pt/BaO/Al_2O_3$ during the NO_2 pulsing experiments is more extensive and apparent than the storage of NO during NO pulsing. For comparison purposes, it is estimated that 10,000 pulses at ca. 4.6×10^{15} molecules/pulse, has an equivalent NO_2 exposure to that of a gas mixture flowing for ca. 205 s at 1 slpm and containing 500 ppm NO_2. With that equivalence established, it is interesting to note that the uptake of NO_2 after 10,000 pulses corresponds to storage of ca. 4.5×10^{-4} mole N/g cat. This is similar in magnitude to the storage measured during the monolith studies (Fig. 7). Nova et al. [24] reported a value of ca. 3.0×10^{-4} mole N/g during NO_2 storage on $Pt/BaO/Al_2O_3$ (1/20/100, w/w).

The evolved NO versus pulse number (Figs. 12 and 13) exhibits the same monotonic increasing dependence observed during the NO_2 storage experiments on the monolith catalysts (Figs. 5 and 6). The plateau at or slightly above the 0.33 level is further evidence for the disproportionation pathway to barium nitrate. More compelling is that the NO evolution occurs with less exposure to NO_2 than during the NO_2 storage experiments at atmospheric pressure: NO breakthrough occurs after only about 200 pulses which is equivalent to about 4 s of flow in the 1 l/min monolith storage experiments. Recall that readsorption of evolved NO downstream in the catalyst bed, leading to <0.33 NO/NO_2 stoichiometry, may explain such a trend [28]. Integral effects encountered during atmospheric pressure storage are not expected to be as significant during high vacuum TAP pulsing experiments. A reduced interaction of evolved NO at lower pressure and the absence of gas phase O_2 makes downstream storage of NO or of NO_2 (via NO oxidation) less likely. Thus, the TAP experiments are able to access the onset of NO evolution more precisely. The period of NO increase at short times is evidence for a mechanism in which NO_2 adsorption/storage leads first to $BaONO_2$ species, followed by liberation of NO with deeper nitration. In the absence of gas phase O_2 this may occur via the overall NO_2 storage mechanisms proposed by Olsson et al. [18,19]. Further discrimination of these mechanisms requires modeling of the NO_2 TAP storage experiments.

5. Conclusions

This study provides new data and insight into the storage of NO and NO_2 on $Pt/Ba/Al_2O_3$ catalysts used for NO_X storage and reduction. We have carried out systematic storage studies for a series of $Pt/BaO/Al_2O_3$ washcoated monolith catalysts with variable Pt loading. The transient storage of NO/O_2 and NO_2/O_2 feed mixtures over a range of exposure times reveal the important enhancing role of Pt as well as similarities and differences in the uptake of NO and NO_2. The trends in the data are consistent with the concurrent pathways of NO_X storage; specifically, the ''nitrite'' pathway and the ''nitrate'' or ''disproportionation'' pathway, both of which have been proposed in the literature.

The short-time storage data indicates that NO and NO_2 store at similar rates in the presence of O_2. This suggests a common rate limiting step or group of steps. The implication from a NO_X storage and reduction modeling standpoint is that the assumption of a single ''NO_X'' species during storage may be sufficient if the storage times are short.

The enhanced storage of NO_2 at longer times indicates the importance of the disproportionation pathway, but the persistence of Pt enhancement suggests that as many as three storage pathways occur concurrently. The first two are the ''nitrate'' or ''disproportionation'' pathway and the ''nitrite'' pathway, while the third is a hybrid pathway involving oxygen on Pt adspecies spillover to BaO followed by uptake of NO_2.

Platinum provides three key functions during NO_X storage. First, Pt catalyzes the oxidation of NO to NO_2, which stores on BaO either by spillover to barium sites in close proximity or by transport through the gas phase to sites further removed from Pt. Second, Pt catalyzes the decomposition of NO_2 to NO. At high Pt loadings the negligible difference between NO and NO_2 feeds suggests an equilibration of the gas mixture. Third, Pt is the integral element of the Pt/Ba ''couple'' in which adspecies spillover to BaO. This is the so-called ''nitrite'' storage pathway. The significant enhancement of NO_X storage is most apparent at low Pt loadings, with enhancement even of NO_2 storage (in O_2), and the correlation of storage capacity with Pt

dispersion (or Pt/BaO interfacial area), all point to the importance of the Pt/Ba couple.

Finally, for the first time TAP data are reported for NO and NO_2 storage on $Pt/BaO/Al_2O_3$. The data reveal a complex picture involving the adsorption and decomposition of NO or NO_2 on the Pt. The TAP data provide evidence for NO and NO_2 uptake on the BaO as well as supporting evidence for a surface NO_X species during the early stages of the process. Additional TAP studies with modeling are needed to further discriminate between these pathways and to estimate kinetic parameters.

Acknowledgements

This research was supported by the Environmental Institute of Houston, the Advanced Technology Program of the State of Texas, and Engelhard Corporation. MH acknowledges helpful discussions with Drs. S. Roth and Y. Li (Engelhard Inc.) and Dr. V. Balakotaiah (UH).

References

[1] N. Miyoshi, S. Matsumoto, K. Katoh, T. Tanaka, J. Harada, N. Takahashi, K. Yokota, M. Sugiura, K. Kasahara, SAE 950809 (1995) 1361.
[2] N. Takahashi, H. Shinjoh, T. Iijima, T. Suzuki, K. Yamazaki, K. Yokota, H. Suzuki, N. Miyoshi, S. Matsumoto, T. Tanizawa, T. Tanaka, S. Tateishi, K. Kasahara, Catal. Today 27 (1996) 63.
[3] W. Bogner, M. Kramer, B. Krutzch, S. Pischinger, D. Voigtlander, G. Wenninger, F. Wirbeleit, M.S. Brogan, R.J. Brisley, D.E. Webster, Appl. Catal. B: Environ. 7 (1995) 153.
[4] P. Han, Y. Lee, S. Han, H. Rhee, Top. Catal. 16/17 (2001) 165.
[5] T. Nakatsuji, V. Komppa, Catal. Today 75 (2002) 407.
[6] J.R. Theis, J.A. Ura, J.J. Li, G.G. Surnilla, J.M. Roth, C.T.J. Goralski, SAE 2003-01-1159 (2003) 5.
[7] W.S. Epling, G.C. Campbell, J.E. Parks, Catal. Lett. 90 (2003) 45.
[8] R. Muncrief, K. Kabin, M.P. Harold, AIChE J. 50 (2004) 2526.
[9] K. Kabin, R. Muncrief, M.P. Harold, Catal. Today 96 (2004) 79.
[10] K. Kabin, R. Muncrief, M.P. Harold, Y. Li, Chem. Eng. Sci. 59 (2004) 5319.
[11] R. Burch, T.C. Watling, The difference between alkanes and alkenes in the reduction of NO by hydrocarbons over Pt catalysts under lean-burn conditions, Catal. Lett. 43 (1997) 19–23.
[12] K.L. Roberts, M.D. Amiridis, Ind. Eng. Chem. Res. 36 (1997) 3528.
[13] D.K. Captain, K.L. Roberts, M.D. Amiridis, Catal. Today 42 (1998) 93.
[14] W.S. Epling, L.E. Campbell, A. Yezerets, N.W. Currier, J.E. Parks II, Catal. Rev.—Sci. Eng. 46 (2004) 163.
[15] H. Mahzoul, J.F. Brilhac, P. Gilot, Appl. Catal. B: Environ. 20 (1999) 47.
[16] E. Fridell, M. Skoglundh, S. Johansson, B. Westerberg, A. Torncrona, G. Smedler, in: N. Kruse, A. Frennet, J.-M. Bastin (Eds.), Proceedings of the Fourth International Symposium on Catalysis and Automotive Pollution Control IV, vol. 116, Elsevier, Brussels, 1997, p. 537.
[17] E. Fridell, M. Skoglundh, B. Westerberg, S. Johansson, G. Smedler, J. Catal. 183 (1999) 196.
[18] L. Olsson, E. Fridell, M. Skoglundh, B. Andersson, Catal. Today 73 (2002) 263.
[19] L. Olsson, H. Persson, E. Fridell, M. Skoglundh, B. Andersson, J. Phys. Chem. B. 105 (2001) 6895.
[20] L. Lietti, P. Forzatti, I. Nova, E. Tronconi, J. Catal. 204 (2001) 175.
[21] F. Prinetto, G. Ghiotti, I. Nova, L. Lietti, E. Tronconi, P. Forzatti, J. Phys. Chem. 105 (2001) 12732.
[22] I. Nova, L. Castoldi, L. Lietti, E. Tronconi, P. Forzatti, Catal. Today 75 (2002) 431.
[23] F. Prinetto, G. Ghiotti, I. Nova, L. Castoldi, L. Lietti, E. Tronconi, P. Forzatti, Phys. Chem. Chem. Phys. 5 (2003) 4428.
[24] I. Nova, L. Castoldi, L. Lietti, E. Tronconi, P. Forzatti, F. Prinetto, G. Ghiotti, J. Catal. 222 (2004) 377.
[25] A. Scotti, I. Nova, E. Tronconi, L. Castoldi, L. Lietti, P. Forzatti, Ind. Eng. Chem. Res. 43 (2004) 4522.
[26] A.J. Patterson, D.J. Rosenberg, J.A. Anderson, Stud. Surf. Sci. Catal. 138 (2001) 429.
[27] J.A. Anderson, B. Bachiller-Baeza, M. Fernandez-Garcia, Phys. Chem. Chem. Phys. 5 (2003) 4418.
[28] W.S. Epling, J.E. Parks, G.C. Campbell, A. Yezerets, N.W. Currier, L.E. Campbell, Catal. Today 96 (2004) 21.
[29] C.K. Narula, S.R. Nakouzi, R. Wu, C.T.J. Goralski, L.F.J. Allard, AIChE J. 47 (2001) 744.
[30] L. Castoldi, I. Nova, L. Lietti, P. Forzatti, Catal. Today 96 (2004) 43.
[31] P.J. Schmitz, R.J. Baird, J. Phys. Chem. B 106 (2002) 4172.
[32] C. Hess, J. Lunsford, NO_2 Storage and reduction in barium oxide supported on magnesium oxide studied by in situ Raman spectroscopy, J. Phys. Chem. B 107 (2003) 1982.
[33] C. Hess, J. Lunsford, Mechanism for NO_2 storage in barium oxide on magnesium oxide studied by in situ Raman spectroscopy, J. Phys. Chem. B 106 (2002) 6358.
[34] X. Li, M. Meng, P. Lin, Y. Fu, T. Hu, Y. Xie, J. Zhang, Trans. I. Chem. E. 80 (2002) 190.
[35] P. Stone, M. Ishii, M. Bowker, Surf. Sci. 537 (2003) 179.
[36] U. Tuttlies, V. Schmeisser, G. Eigenberger, Chem. Eng. Sci. 59 (2004) 4731.
[37] R. Muncrief, P. Khanna, K. Kabin, M.P. Harold, Catal. Today 98 (2004) 393.
[38] K. Kabin, R. Muncrief, M.P. Harold, Y. Li, Chem. Eng. Sci. 59 (2004) 5319.
[39] J.T. Gleaves, J.R. Ebner, T.C. Kuechler, Catal. Rev.—Sci. Eng. 30 (1988) 49.
[40] NIST mass spectrometer database: http://www.msel.nist.gov/.
[41] P. Khanna, M.S. Thesis, University of Houston, 2004.
[42] R. Masel, Catal. Rev.—Sci. Eng. 28 (1986) 335.
[43] R. Burch, P.J. Millington, A.P. Walker, Appl. Catal. B 4 (1994) 65.
[44] G.P. Ansell, S.E. Golunski, J.W. Hayes, A.P. Walker, R. Burch, P.J. Millington, Stud. Surf. Sci. Catal. 96 (1996) 577.
[45] R. Muncrief, V. Medhekar, M. Harold, Unpublished results, 2002, 2005.